Supplement of Atmos. Chem. Phys., 26, 10241–10253, 2026
https://doi.org/10.5194/acp-26-10241-2026-supplement

Atmospheric Chemistry and Physics
Open Access

Supplement of

Constraining the atmospheric hydrogen oxidation and soil sink seasonal cycles using HFC-152a

Kane Stone et al.

Correspondence to: Kane Stone (stonek@mit.edu)

Text S1.

Arrhenius equations used in the box model for the H_2 and HFC-152a oxidation reactions.

$$H_2 + OH: 2.8 \times 10^{-12} e^{-1800/T}$$

$$HFC152a + OH: 2.4 \times 10^{-12} e^{-1260/T}$$

Table S1. ERA5 monthly average temperatures from the surface to 200 hPa and monthly diffusive transport terms used in each box.

Temperature - North (K)	Temperature - Tropics (K)	Temperature - South (K)	Diffusive transport - North – Tropics ($days^{-1}$)	Diffusive transport - South – Tropics ($days^{-1}$)
253.2	271.6	260.8	120.4	154.0
253.3	271.8	260.9	120.4	154.0
255.8	272.0	259.6	219.1	154.0
258.7	272.2	257.7	219.1	245.7
261.4	272.3	255.8	219.1	245.7
265.4	272.0	254.3	141.4	122.5
268.7	271.7	253.6	141.4	122.5
267.2	271.7	253.5	141.4	122.5
264.4	271.8	254.2	221.2	233.8
261.6	271.8	255.5	221.2	233.8
257.7	271.7	257.5	221.2	233.8
254.3	271.6	259.5	120.4	154.0

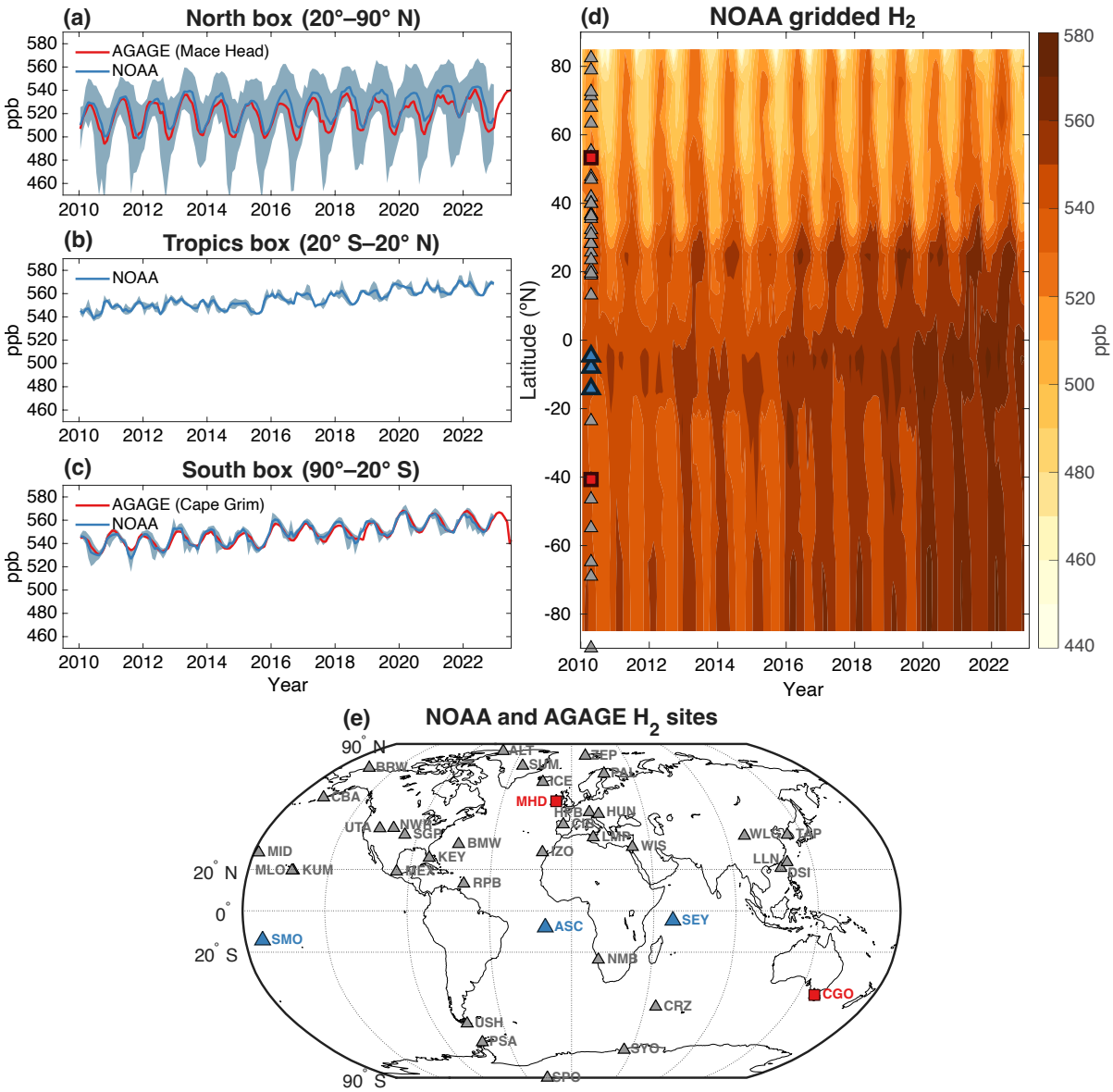

Figure S1. Comparison of (a) Mace Head and (c) Kennaook/Cape Grim H_2 data with North and South box average and range (shaded region) of NOAA flask-air data over 2010–2022. Average Tropics box NOAA data is shown in (b) based on stations at the blue triangles in (d). A linearly filled latitude-time NOAA dataset is shown in (d). Gray triangles show the latitudes of NOAA sites (https://gml.noaa.gov/dv/site/?program=ccgg). Red squares show the location of Mace Head and Cape Grim AGAGE sites.

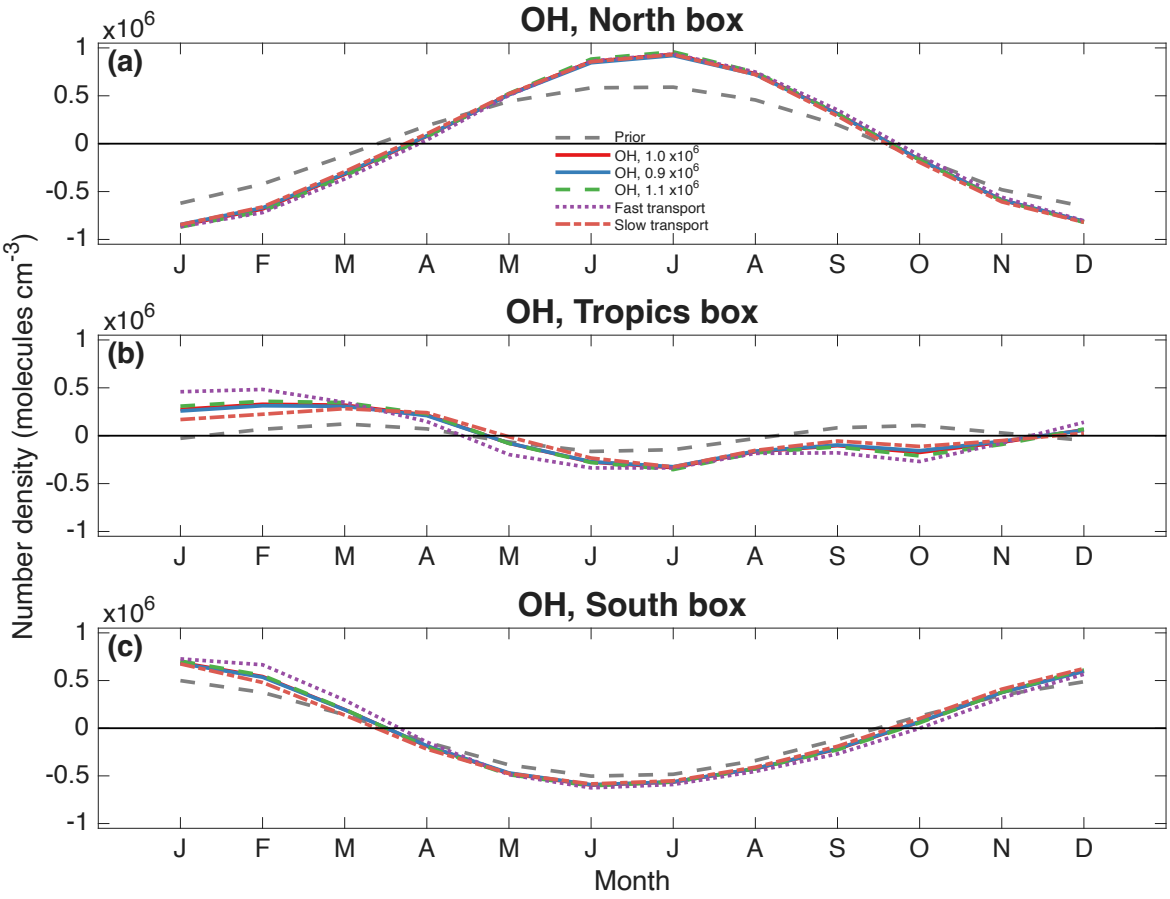

Figure S2. Optimized OH mean seasonal cycle when using different prior OH absolute values and 30% faster or slower diffusive transport terms for the (a) North box, (b) Tropics box, and (c) South box.

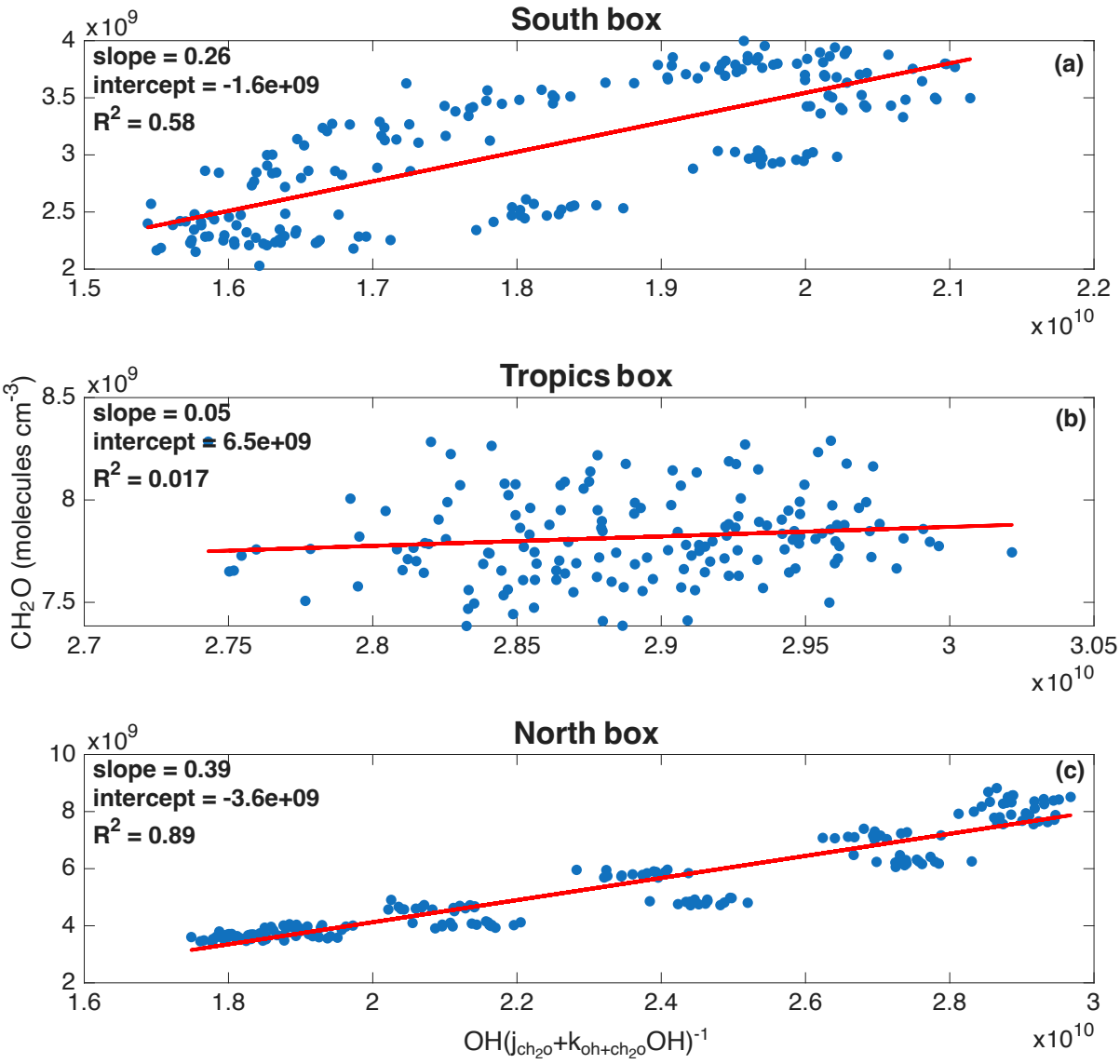

25

Figure S3. Model and TROPESS reanalysis derived slope and intercept terms for the (a) South box, (b) Tropics box, and (c) North box for the CH_2O derived from OH case following Eq. 1 in the main text.

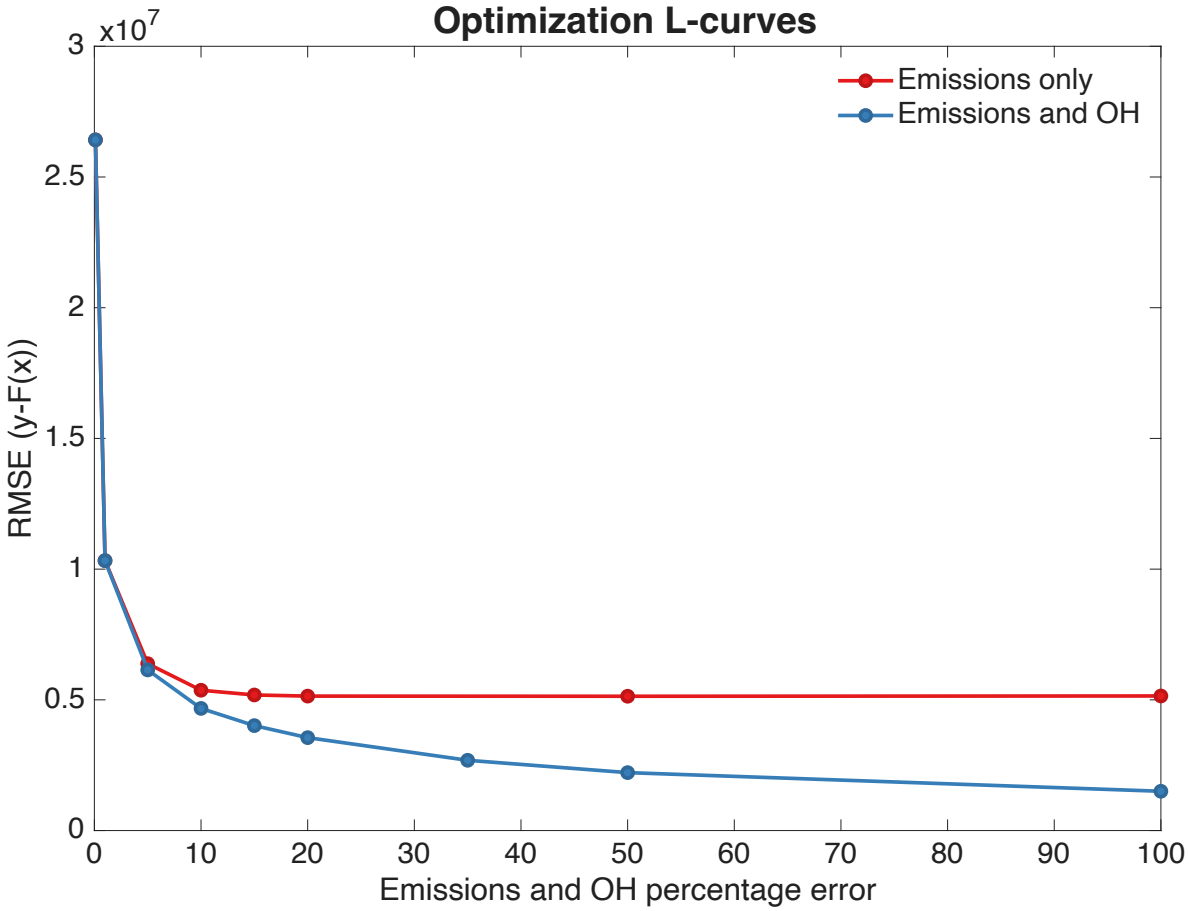

Figure S4. Optimization L-curves for the prior error covariance matrices of HFC-152a. For emissions only, OH error was set constant at 0.1%. For emissions and OH, both emissions and OH varied together.

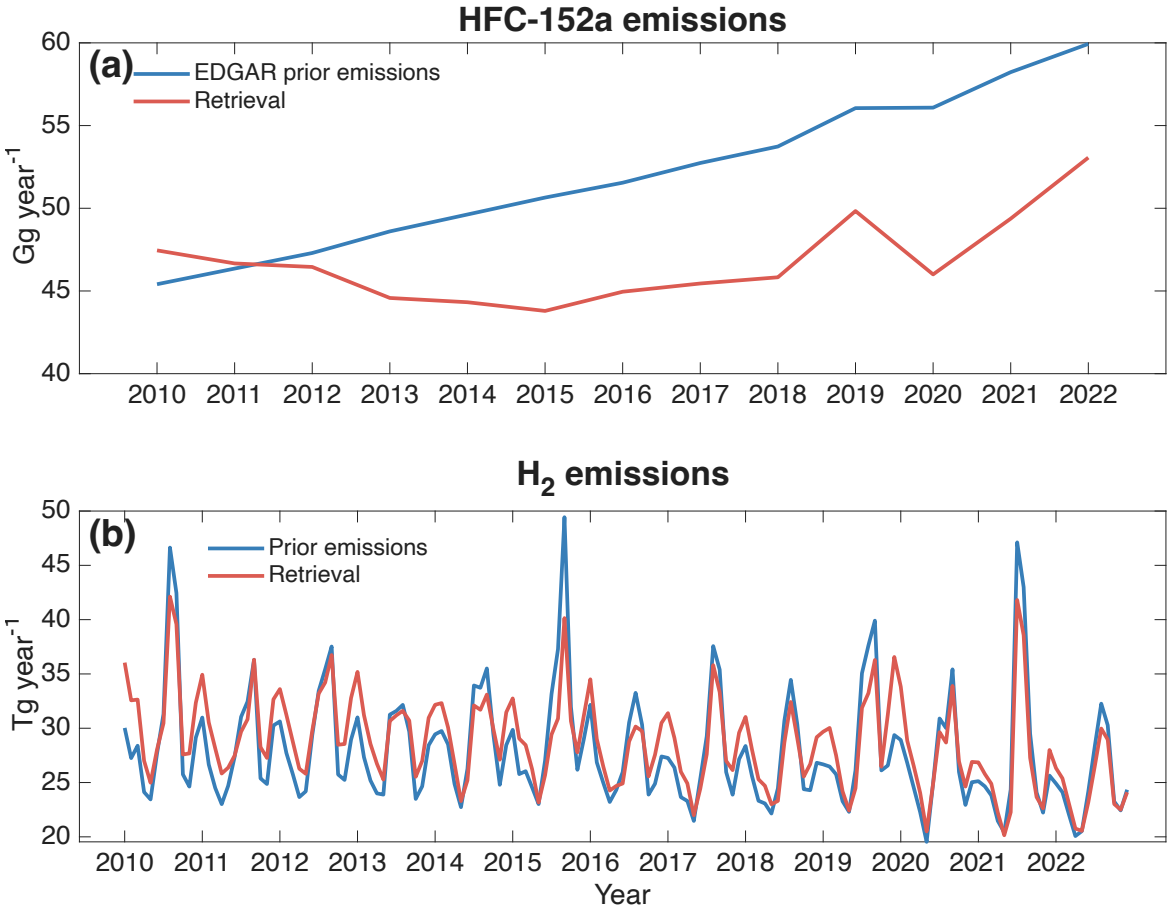

Figure S5. Retrieval of yearly HFC-152a emissions (a), and monthly H_2 emissions (b) for case 1 (see main text).

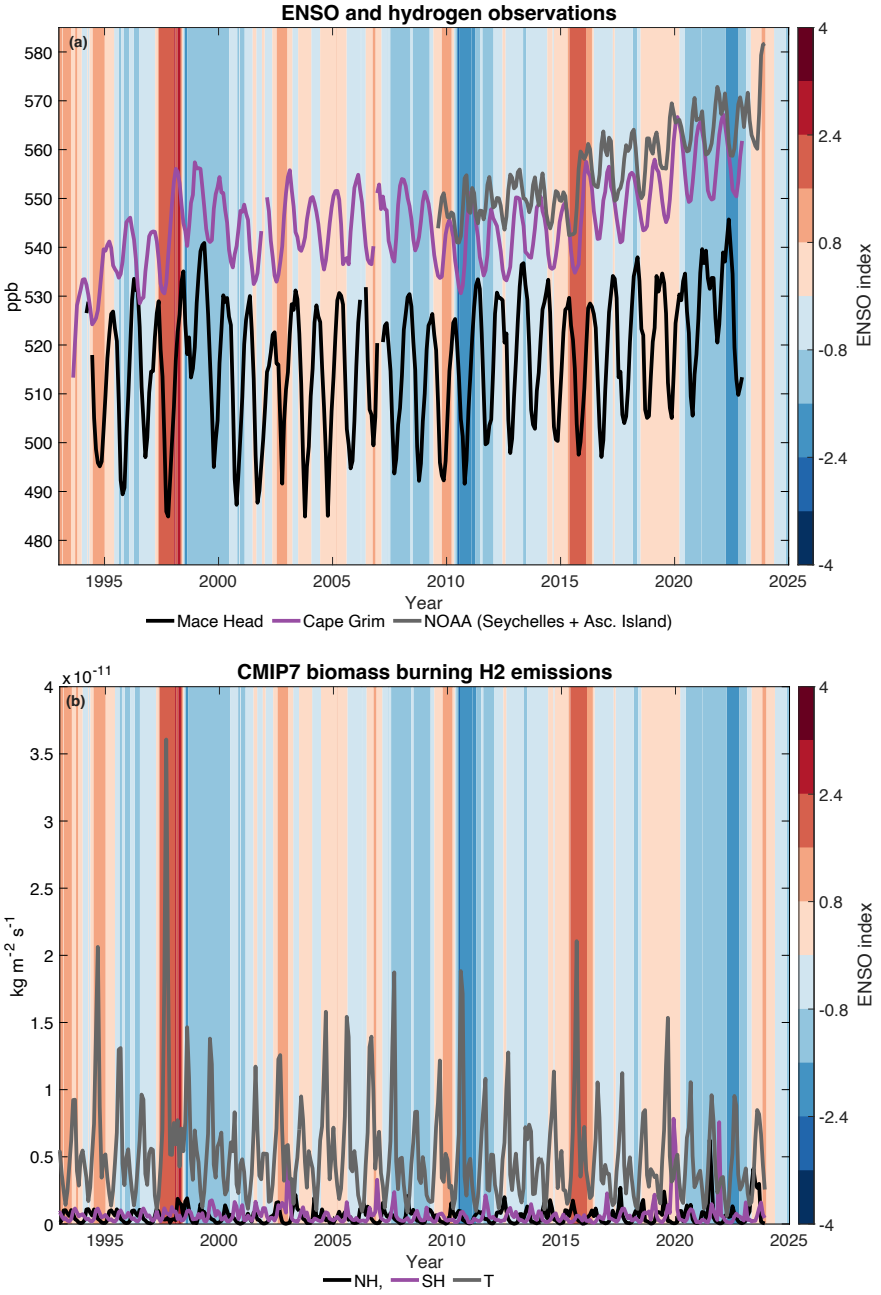

Figure S6. (a) AGAGE and NOAA observations of H_2, and (b) CMIP7 biomass burning H_2 emissions overlaid on the ENSO index from MEI v2 (Wolter and Timlin, 2011; https://psl.noaa.gov/enso/mei/, last accessed 2025/11/04).

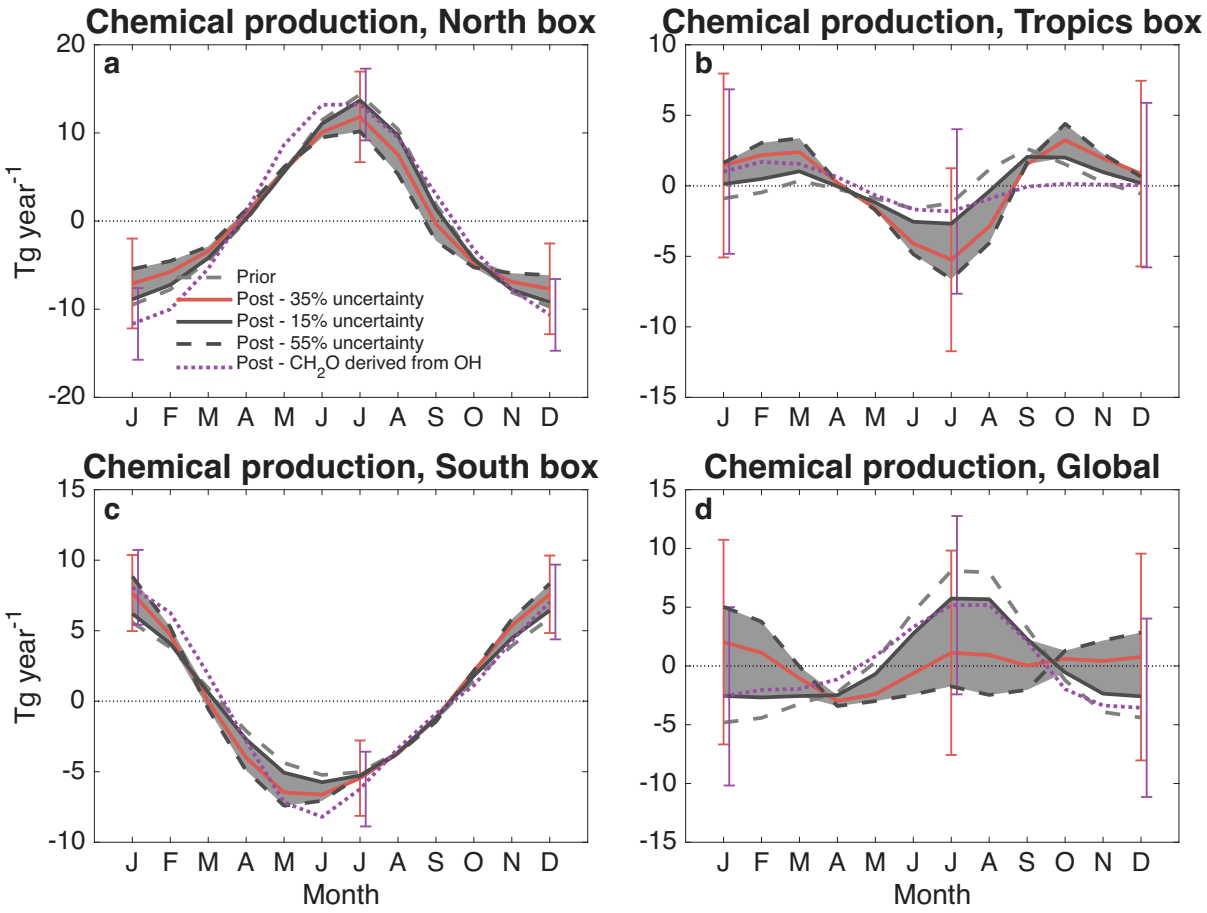

Figure S7. Monthly anomalies of H_2 chemical production from the yearly mean for all cases in (a) the North box, (b) the Tropics box, (c) the South box, and (d) globally. The shaded region shows the range between the 15%, 35%, and 55% uncertainty cases (see Table 1 in main text). The CH_2O derived from OH case (dotted line) is also shown. The error bars for the 35% uncertainty case show the retrieved posterior standard deviation uncertainty. The error bars for the CH_2O derived from OH case are estimated from the retrieved OH posterior standard deviation uncertainty and shown for select months of January, July, and December. The grey dashed line shows the prior estimate for the chemical production in each box. Results are averaged over the 2010–2022 time series.

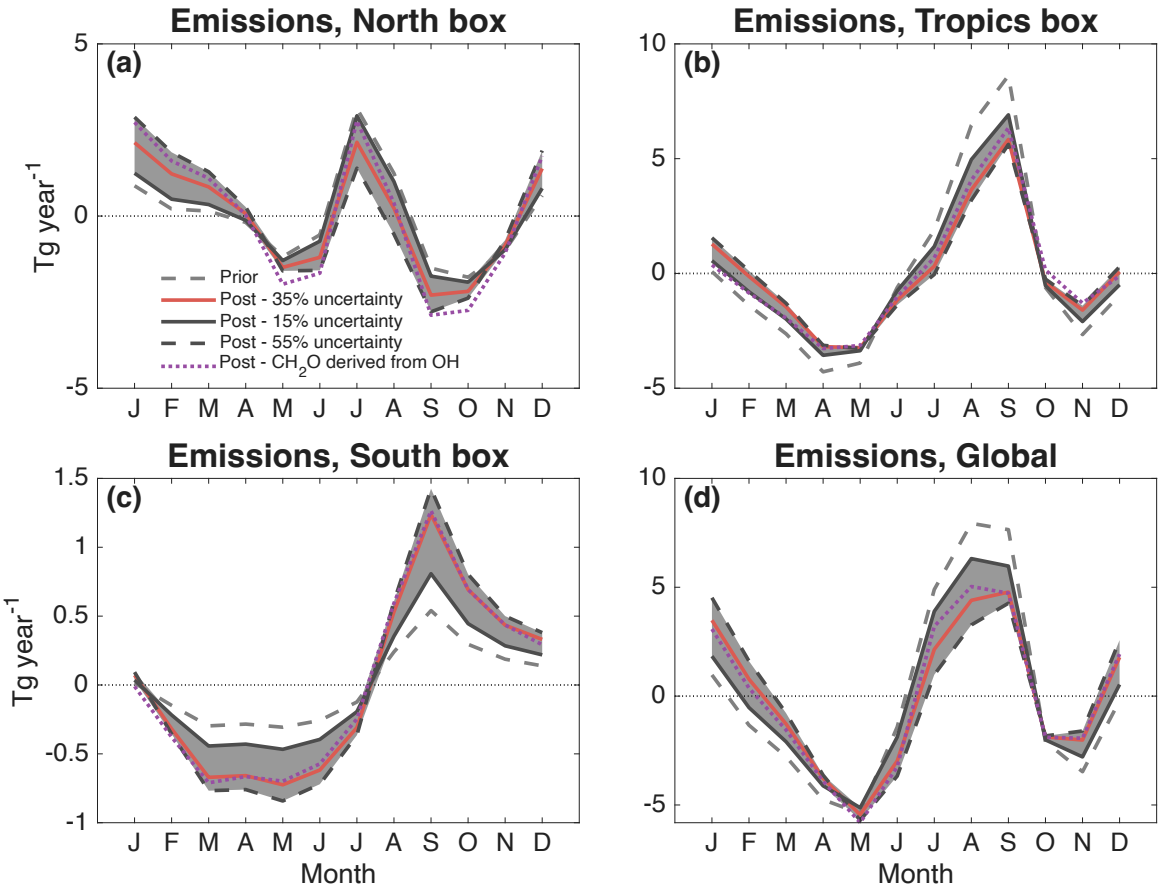

Figure S8. Same as Figure S7, but for H_2 emissions.

References

Wolter, K. and Timlin, M. S.: El Niño/Southern Oscillation behaviour since 1871 as diagnosed in an extended multivariate ENSO index (MEI.ext), Intl Journal of Climatology, 31, 1074–1087, https://doi.org/10.1002/joc.2336, 2011.